Microfluidics and Nanofluidics (2019) 23:4
https://doi.org/10.1007/s10404-018-2170-1

RESEARCH PAPER

Sperm-like-particle (SLP) behavior in curved microfluidic channels

Jiyoung Son[1] · Alexander R. Jafek[2] · Douglas T. Carrell[3] · James M. Hotaling[3] · Bruce K. Gale[2]

Received: 12 June 2018 / Accepted: 24 November 2018 / Published online: 3 December 2018

Abstract
Microfluidic technology has the potential to separate sperm cells from unwanted debris commonly found in clinical samples while improving the effectiveness of assisted reproductive technologies. In this study, we present an improved model of sperm cell behavior in curved channels based on both 2D COMSOL® simulations and experimental studies. The 2D COMSOL® simulation results show alignment of the sperm like particles, which suggests that sperm should be treated as small, relatively stationary particles rather than larger rotating particles. This understanding helps us generate more precise sperm separations for μTESE samples by enabling the assumption of a small particle rather than a large one. This alignment was also confirmed by observing the alignment angle of all recognizable sperm cells with high-speed imaging near the outlet area of the spiral channel. A series of experiments with sperm cells and microbeads showed clear separation improvement between the new experimental conditions and previous efforts. Sperm were found to behave more similarly to 3 μm beads than to 5 μm beads and that sperm cells may act like particles even smaller than the 3-μm beads. The focused sperm cell stream appeared in the middle area of the channel and the focused RBCs stream appeared at the mid-inner wall area of the channel. Basic biocompatibility testing also suggests that the approach can be used safely in a clinical setting.

1 Introduction

In recent biological studies, focus has shifted from broad genetic analysis to individual cell biology as differences in individual cells are being explored to enhance our biological understanding. At the single cell level, it has been challenging to make measurements, because cell samples are highly complex and contain many different species at widely different abundance levels (Shields et al. 2015; Kim et al. 2008; Andersson and Berg 2003). Therefore, the ability to sort and separate individual cells or cell types has become particularly important and using microfluidic technology has proven a favorable solution due its inherent capabilities at this scale for automation and high throughput (Shields et al. 2015; Bhagat et al. 2010; Nagrath et al. 2007; Nam et al. 2012; Gossett 2010). Microfluidic approaches have been applied specifically in male fertility studies to separate motile sperm cells from unwanted debris and to improve the efficiency of assisted reproductive technologies (ART) (Swain et al. 2013). A current popular microfluidic approach for sperm separation utilizes parallel laminar fluid streams of media through a straight microchannel: one stream consisting of a dilute semen sample, and the other stream consisting of sperm media (Cho et al. 2003; Schuster et al. 2003). At the micro scale, the two fluid streams do not mix readily such that only motile sperm, responding to a flow or shear stress, can travel across the interface between the two parallel streams. The two streams are separated again after a length sufficient to allow motile sperm to separate from non-motile sperm and debris. This, and other microfluidic sperm separation approaches, used until now, have been heavily reliant on sperm motility, employing microchannel features such as laminar flow with chemo-attractants (Xie 2010; Koyama et al. 2006a, b; Ko et al. 2012), physical obstacles (Suh et al. 2006), and micro-diffusers (Lin et al. 2013). Since these methods were only designed to collect progressive motile sperm cells from semen samples, they lose a significant number of viable sperm cells including non-progressive

Electronic supplementary material The online version of this article (https://doi.org/10.1007/s10404-018-2170-1) contains supplementary material, which is available to authorized users.

✉ Jiyoung Son
smirage9@gmail.com

[1] Electrical and Computer Engineering, University of Utah, Salt Lake City, USA

[2] Mechanical Engineering of University of Utah, Salt Lake City, USA

[3] Urology Division of Department of Surgery, University of Utah School of Medicine, Salt Lake City, USA

motile and non-motile sperm cells. For patients with low quantities of low-quality sperm, these approaches are not optimal as they select against the patient's immature and non-motile sperm cells despite the fact that those cells could have the potential for conception using ICSI.

Recently, we demonstrated sperm separation utilizing a spiral channel for simulated testicular sperm extraction (TESE) and microdissection testicular sperm extraction (μTESE) samples which include not only sperm cells, but also red blood cells (RBC), white blood cells (WBC), and other contaminating debris (Son et al. 2015, 2017). This study showed purely mechanical, label-free separation of sperm from a simulated μTESE sample using inertial microfluidics. The approach did not require any externally applied forces except the movement of the fluid sample through the instrument. Using this method, we were able to recover not only motile sperm, but also viable less-motile and non-motile sperm at a high recovery rate. This separation was achieved primarily by focusing RBCs to a consistent location in the channel and then collecting the unwanted cells away from the sperm cells, while only generating a slight hint of sperm focusing. Although performing the separation in this way was an important step forward, and represented a significant contribution to the field, an optimized microfluidic inertial focusing system would generate sharp flow focusing of both RBCs and sperm cells at different locations. This type of system would represent an important improvement, because it would increase our confidence that all sperm cells were selected and allow us to make that selection more precisely.

Our hypothesis is that sharp flow focusing of sperm cells would be enabled through a better understanding of sperm behavior in the curved channel. Specifically, we hypothesize that an improved understanding of the dynamic forces felt by the non-spherical sperm cells is necessary to more reliably predict and then control their behavior. The general theory of inertial focusing assumes that the target particle is spherical; however, in live cell samples [such as sperm cells, RBCs, and WBCs (Son et al. 2017; Hur et al. 2011; Amini et al. 2014)] this is rarely the case. In a study to understand the behavior of non-spherical shaped particles within a microchannel (Hur et al. 2011), it was shown that the particles rotated as they moved through the channel and that their focusing behavior could be characterized utilizing their rotational diameter. For sperm cells in particular though, this simplification is particularly suspect because of the long tail, which would inhibit continuous rotation as occurs with other non-spherical particles.

In this study, we develop an improved model of sperm cell behavior in curved channels based on both 2D COMSOL® simulations and experimental studies. The purpose of the study was to find the behavior of a sperm-like-particle (SLP) within a curved channel and use this knowledge to improve our ability to focus sperm. Our results show that a SLP has an inherent tendency to align in the direction of the primary flow. Using this understanding we calculate new focusing conditions, which significantly improve flow focusing of sperm within the previously designed spiral channel (Son et al. 2015, 2017). The results show promising evidence that the proposed method should be able to generate more precise sperm separation for μTESE samples.

2 Known design theory and challenges

Previous studies of inertial effects have presented the physical design guidelines for generating flow focusing of target particles in a spiral channel (Amini et al. 2014; Martel and Toner 2012, 2013; Zhou and Papautsky 2013). The guidelines include the following group of non-dimensional parameters: the force ratio (R_f), the ratio of particle diameter and channel hydraulic diameter (λ), and the aspect ratio of the channel. The force ratio (R_f) (Eq. 1) is a ratio between the Dean drag force (F_D) (Eq. 2) and the net lift force (F_L) (Eq. 3), where F_D is the force resulting from a secondary vortex that appears laterally in the curved channel and F_L represents the combination of wall effect lift and shear gradient lift force (Amini et al. 2014; Martel and Toner 2012, 2013; Zhou and Papautsky 2013). According to the guidelines, R_f should be greater than 0.08 and λ should be more than 0.07. The aspect ratio of the channel should be between approximately 1:2 and 1:4 (height: width) (Son et al. 2015, 2017):

$$R_f = \frac{F_L}{F_D} \geq \sim 0.08, \tag{1}$$

$$F_D = 3\pi\mu U_{Dean} a_p, \tag{2}$$

$$F_L = 0.05 \frac{a_p^4 \rho U_m^2}{D_h^2}. \tag{3}$$

In these equations, μ is fluid viscosity, U_{Dean} is the average Dean velocity, a_p is particle diameter, ρ is the density of the fluid (water), D_h is the hydraulic diameter, and U_m is the maximum fluid velocity.

While this theory is well established, it assumes spherical particles, and when used with nonspherical particles (such as many types of cells) it requires the assumption of a representative diameter. Since this simplification has a significant impact on design guideline (F_D, F_L), it has been a critical consideration for those designing spiral channels. Hur et al. (2011) suggested the use of the rotational diameter of the particle since most particles rotate while they travel through the microchannel in laminar flow

and reported that the rotational diameter of the particle (regardless of its cross-section shape) could determine the final focused position in most of cases. Based on this finding, the behavior of symmetrical, non-spherical cells has been approximated using the rotational diameter or the largest diameter of the cell (Bhagat et al. 2011; Lee et al. 2013; Mach and Carlo 2010). In our previous report, we also utilized Hur's suggestion, using the rotational diameter to predict the focusing of target particles in inertial equations (Son et al. 2015, 2017). The sperm cell, which is composed of an ellipsoid head (~ 5 μm length, ~ 3 μm width) and a long, flexible tail (30–49 μm length) was assumed to behave as a rotating sphere of diameter 5 μm (Mossman et al. 2013), and RBCs, which are biconcave disks of ~ 9 μm diameter, were assumed to behave as rotating spheres of diameter 9 μm (Diez-Silva et al. 2010; Guz et al. 2014). The longest dimension of a normal morphology sperm head (5 μm) was utilized as a simplified sphere diameter while 9 μm, and 12 μm diameter spheres were utilized as models for RBCs and WBCs, respectively. After a series of calculations based on the theory of flow in spiral channels and the assumed dimensions of the particles to be separated, channel dimensions were selected that meet the typical design guidelines: channel height = 50 μm, channel width = 150 μm, space between channels = 310 μm, initial radius of the spiral = 700 μm, final radius of the spiral = 899 μm. In order to make Rf (for 5 μm, 9 μm and 12 μm diameter particles) higher than 0.08, the flow rate of the injected sample should be at least 0.52 ml/min (Son et al. 2015, 2017).

As previously explained, while this spiral channel was able to generate clear, sharp flow focusing of RBCs, the sharp flow focusing of sperm did not appear. The successful flow focusing of RBCs under conditions where a sphere of similar would be focused implies that the spherical model did accurately predict the behavior of RBCs, but the lack of focusing of sperm cells implies that even though the conditions were devised for a spherical particle assumed to be similar to that of a sperm cell, the conditions were not appropriate, suggesting that the model was in some way incorrect. The lack of focusing of sperm may potentially be corrected using the findings of a recent study of aligning behavior of an uneven doublet particle (Uspal et al. 2013). In Uspal's study, the long axis of uneven double particles aligned with the primary flow in the microfluidic channel. This study led us to predict that a sperm cell will also have a tendency to align itself with the flow due to the morphologic similarities with double beads. Using this behavior to help model the behavior of sperm in a channel should be a good foundation to improve modeling and, therefore, focusing of sperm cells in a spiral microfluidic channel.

3 Methodology

In this work, we demonstrate sperm cell alignment through both simulation and experimental data and show how this affects the cell's focusing behavior. We also use this information to improve sperm focusing. Finally, we show experiments using simulated μTESE samples to show a potential application of this phenomenon.

3.1 Sample preparation

Depending on experimental necessity, three types of particles were used: sperm cells, red blood cells, and beads. Sperm cells and red blood cells were acquired and prepared (DAPI, PKH26 stain) as explained previously (Son et al. 2015, 2017) and were acquired as part of an IRB approved study. We also utilized 5 μm (Bangs laboratories, Fluorescent Carboxyl Polymer Microbeads, Red), and 3 μm (Polysciences, Fluoresbrite, Yellow Green) fluorescent microbeads. During device operation, all particles were suspended in Quinn's media at various concentrations (sperm and microbeads: 0.1–1 million/ml, μTESE: ~ 10 million/ml).

3.2 Device protocol and operation

Syringes (BD, 1 ml Syringe Luer-lock tip), manipulated at a rate controlled with syringe pumps (KD Scientific, dual syringe pump 210), were used to inject and withdraw sample from the spiral channel device whose fabrication and operation is explained extensively in our previous report (Son et al. 2015, 2017).

3.3 COMSOL simulation

Two-dimensional (2D) finite element software simulations of SLP dynamics were performed using COMSOL Multiphysics®. 2D simulations were utilized due to the relative simplicity of the study and the reduced computational power that they require. Although 2D models neglect the Dean force-induced secondary vortex flow, according to the Dean force and Dean velocity equations, the lateral particle migration velocity imposed by the Dean force is relatively insignificant compared to the primary flow velocity in terms of magnitude (The Dean velocity is often thousands of times less than the primary flow velocity), so effects caused by the primary flow field should dominate particle behavior. Therefore, the 2D model should provide an appropriate representation of SLP behavior in a curved channel with a relatively high flow rate.

The SLP was modeled to be geometrically slightly shorter than normal sperm cell dimensions (Mossman

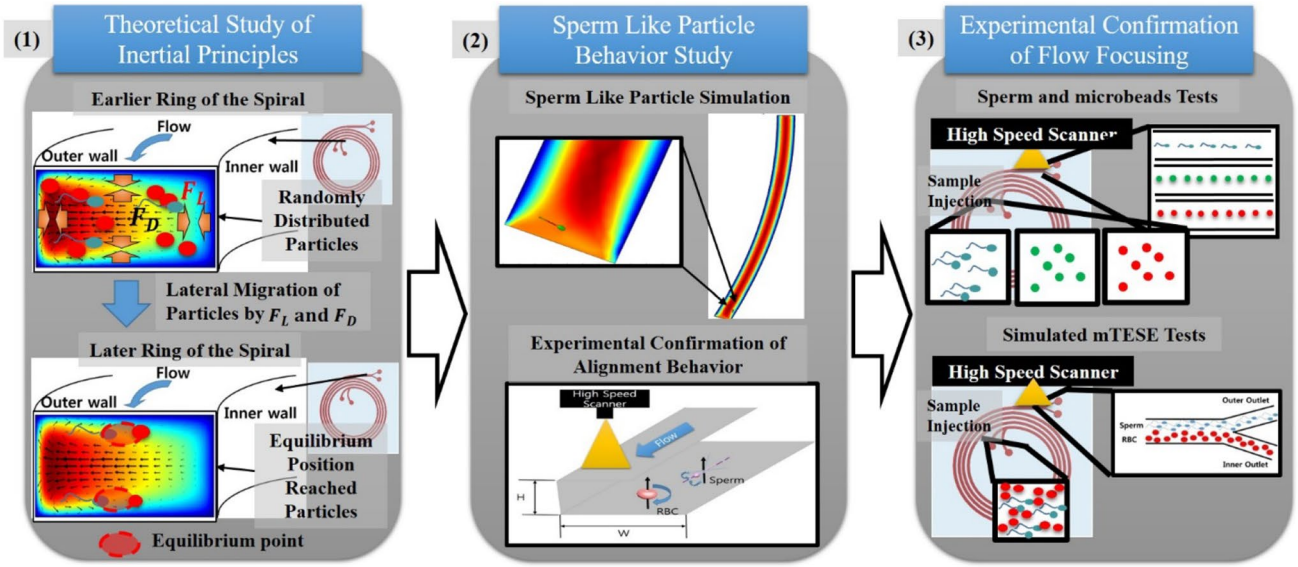

Fig. 1 Overview of the Study, (1) Understanding the impact of the particle behavior within inertial microfluidics principles, (2) SLP behavior study utilizing COMSOL, and experimental confirmation studies enabling an improved solution of SLP modeling, (3) Experimental confirmation studies utilizing sperm, micro-beads, and simulated μTESE samples to show the improvement of flow focusing of sperm cells

et al. 2013), because sperm cells from μTESE samples generally include immature sperm cells. The SLP model contained an ellipsoid head (5 μm length, 3 μm diameter) and a short, extended tail (30 μm long, 1 μm thick). To represent the flexibility of real cells, a Young's modulus of 1.6 kPa was applied to the SLP, which is similar to the Young's modulus of the average cell membrane (Guz et al. 2014). As the behavior of the SLP is most interesting in the initial part of the channel (before it has reached its focus location), only a small, initial portion of the channel was simulated, and the behavior of the particle along this length was used to draw conclusions about the SLP as it travels the length of the channel. Specifically, channel dimensions were obtained from the first 1/16th of the innermost ring of the spiral channel. Thus, the simulated length was 2.86 mm, 150 μm wide, with a 7-mm radius of curvature. The no-slip condition is applied at the fluid boundaries. Fluid (water) was injected with a velocity of 0.14 m/s, and the SLP was given an initial position near the channel inlet (Fig. 2).

To understand the behavior of an SLP with a variety of initial conditions, a total of eight simulations were completed: seven with SLPs placed in the channel with a unique combination of location and orientation as well as an eighth case in which a tail-less sperm head-like particle in the curved channel was used as a control against which to compare the results of the SLP simulations. The initial position of the particles were parameterized by the initial location of the head (as measured from the inner wall) and the orientation was parameterized by the alignment of the tail relative

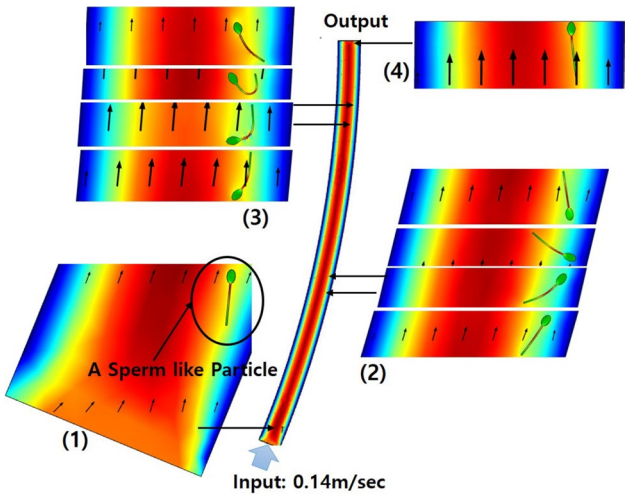

Fig. 2 An example of 2D COMSOL® simulations completed in this work, (1) initial position of the SLP, (2) the first rotation of the SLP, (3) the second rotation of the SLP, (4) the final position of the SLP

to the direction of the primary flow. Figure 3 shows that initial condition of the eight simulated cases.

We quantified the movement of the SLP through the length of the channel across the following variables: total travel time, number of 360° rotations completed, percent of the time (and distance) that the particle spent rotating, and the percent of the time (and distance) that the particle spent aligned. The final alignment and location of the particle were also quantified with the same metrics that quantified the SLP's initial position.

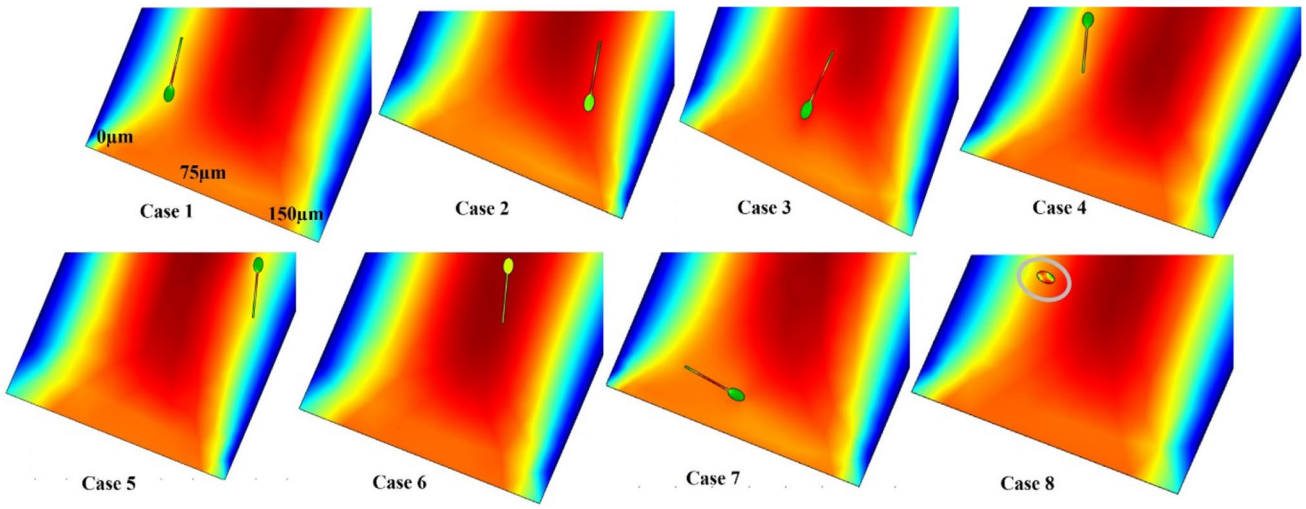

Fig. 3 2D COMSOL simulations for SLPs in eight different initial positions

3.4 Experimental verification of the simulation

To verify the COMSOL simulation results experimentally, individual sperm cells were tracked in a spiral channel system. To observe the alignment of various sperm cells, a Nikon AR1 inverted microscope with a high-speed scanner (230 frames/s) was utilized to observe the alignment of various sperm cells (Figs. 1, 2). The selected area near the outlet of the spiral channel was recorded while DAPI-stained sperm cells were injected through the channel. The sperm sample concentration was between 0.1 and 1 million/ml. The injection flow rate was 0.3 ml/min (0.67 m/s), which was the highest possible flow rate that allowed sperm identification in a frame. The recorded files were accumulated over 5 min. The DAPI blue stained sperm head and tail were clear identification factors allowing us to distinguish sperm from other particles. From the videos, 102 sperm cells were identified for alignment angle measurement. ImageJ was used to measure the alignment angle between sperm cells and the primary flow direction.

3.5 Employing a new SLP model

The simulation study and the experimental confirmation provided new understanding and evidence of the SLP self-alignment behavior within the spiral channel and showed that sperm cells do not continuously rotate as do the other non-spherical particles as reported as Hur's study (Hur et al. 2011). The observed behavior of the SLPs provided evidence to justify changing the sperm modeling assumptions, specifically by selecting a new representative particle diameter (a_p). Since SLPs are mostly aligned in either a head lead or tail lead position, the two essential lateral particle migrating forces (F_D and F_L) will mostly effect the non-rotating side surface of the sperm heads and which are not well-represented by a 5-µm diameter sphere. This result suggests a reduction of the lateral force effect surface area of the particle, which means assuming a new smaller value of a_p in the force (F_D and F_L) equations.

Since the new sperm cell model assumes a reduced force effect area of the sperm head compared to the previous estimation, the width of sperm head (3 µm) can be selected as a more conservative particle model diameter (a_p) than the longer axis of a sperm head (5 µm). Therefore, the head width dimension was taken as a new a_p and used in Eqs. 2 and 3. With a new a_p and the current spiral channel dimensions, the minimum flow rate to reach $R_f > 0.08$ for sperm cells was calculated to be 1.725 ml/min (3.83 m/s).

A set of experiments was designed to verify the new minimum condition for focusing sperm in a spiral channel. The experiments included tests of three types of particles: DAPI stained sperm, 5 µm (red), and 3 µm (green) fluorescent microbeads, at three different flow rates: 014.52 (1.15), 1.04 (2.31), and 1.7 ml/min (3.83 m/s). These tests allowed us to observe the changes in flow focusing of each particle with varied flow velocities. The utilized flow rate of 1.7 ml/min was slightly lower than the calculated flow rate of 1.725 ml/min, but was utilized to prevent possible damage of the experimental setup due to the high pressure required. The two sizes of microbeads represent the two models of the sperm head. Specifically, the red, 5 µm bead represents a rotating sperm cell using the longest head length and the green 3 µm bead represents the non-rotating sperm using the sperm head width as the diameter of the spherical particle models. The flow rate of 0.52 ml/min represents the flow rate calculated from ~ 5 µm sphere modeling and the flow rate of 1.7 ml/min represented calculated flow rate based on ~ 3 µm sphere modeling. The flow rate of 1.04 ml/min is added to

show the flow focusing pattern change as the flow rate is increased. With the same high-speed microscopy set-up from our previous work (Son et al. 2015, 2017) videos were recorded for 6–8 s (~ 1800 frames) and the video frames were projected into an image to show traces of all particles. As before, videos were taken near the outlet of the spiral channel. The intensity profile of each projected images was extracted by NIS Elements software and plotted in Excel. A normalized summation of the different images was generated to allow comparison graphically of the location of the peaks. Note that this approach is inherently non-quantitative as the fluorescence is not calibrated and many of the images had saturated regions. Still, the results give a reasonable representation of where the particles are located in the channel.

3.6 Application of the new SLP model for µTESE

To demonstrate the usefulness of this new method for processing µTESE samples, a set of experiments was designed to verify the focusing improvement effect of the new flow rate condition with simulated µTESE samples. Utilizing the same flow rates used in the other experiments (0.52, 1.04, and 1.7 ml/min), these tests allowed us to observe the changes in flow focusing of sperm cells and RBCs with varied flow velocities. The flow rate of 0.52 ml/min represents the flow rate calculated from ~ 5 µm sphere modeling and the flow rate of 1.7 ml/min represented calculated flow rate based on ~ 3 µm sphere modeling. The flow rate of 1.04 ml/min is added to show the flow focusing pattern change of each particle while the flow rate is increased. The data acquisition protocols for tests with simulated µTESE samples were the same as above, except the number of frames used for projection images was reduced to ~ 100 frames because of the higher concentration of particles in the flow. Specifically, RBCs had a concentration of ~ 10 million/ml, while the concentration of sperm cells was between 0.1 and 1 million/ml which is different from the typical clinical µTESE sample. The RBC concentration of the simulated sample is much lower than the clinical samples because particle concentrations that are too high inhibit the effects of the inertial focusing, so the RBC samples were diluted, and dilution may be required for practical application of this work. In addition, to visualize sperm cell behavior with the simulated sample, it was necessary to have a higher concentration of sperm cells than is found in a typical clinical µTESE sample (Son et al. 2015, 2017).

3.7 Clinical safety verification

As data from this study were used to propose a tool that is meant for clinical application, we performed both a live/dead test and morphology test (the most common clinical methods to verify sperm quality) on processed sperm. For both tests we utilized the standard WHO protocol (WHO 2010) for test and sperm sample reading protocols. Samples from two different patients were used.

4 Results and discussion

4.1 Simulation results: sperm alignment

Our simulations verify that unlike the rotational behavior of non-spherical particles which have been previously studied (Hur et al. 2011), the SLPs have a tendency to align with the primary flow in either a tail lead or head lead position and show a strong resistance to rotation. Aligned particle behavior was observed during almost the entirety of every SLP's travel through the channel (84–100%) and was not observed at all in the case of the tail-less particle (Case 8). In terms of rotations, two cases (Case 3 and 6) showed no rotation and in cases where the SLP did rotate, rotations were quicker and shorter than in the tailless particle case (Fig. 3, case 8). Even in Case 1 where three rotations were observed, these rotations happen over just 13% of the channel's distance. This result is nearly the opposite of that observed for the tailless particle, which tumbled throughout the entirety of its travel through the curved channel. In every case, the length of the channel that the particle spent rotating was very short compared to the overall particle travel distance (Table 1).

The possible cause for the rotation is a combination of the parabolic flow velocity profile of the channel- and wall-induced lift force (Fig. 4). When a SLP is located between multiple boundaries of clearly different velocity fields (Fig. 3, case 1, case 2, case 4, case 5, and case 7), the higher velocity pushes the closest edge of the SLP, which causes a rotation (Figs. 2-2, 3) or a self-alignment.

The alignment phenomenon can also be explained in terms of the particle's location and orientation relative to the flow velocity profile. When the particle is located mostly in the higher velocity field (Fig. 3, red color velocity profile area) in the middle of the channel (Fig. 3, Case 3, Case 6), the particle alignment is maintained as the particle is exposed to a minimal difference between neighboring streamlines across the edges of the particle. This type of particle behavior should be more dominant in the later rings of the spiral channel because particles should migrate to a stable equilibrium area (upper and bottom middle are of the channel, Fig. 1-1) of the rectangular channel as the shear gradient lift force and wall effect lift force balance (Amini et al. 2014). This also means that there should not be any rotation of SLPs relative to the flow field in the later rings of the spiral channel.

Table 1 2D simulation summary table

Case #	1	2	3	4	5	6	7	8
Initial location of head[a]	30 μm	100 μm	72 μm	30 μm	110 μm	75 μm	75 μm	35 μm
Initial alignment with θ[b]	Tail lead (190°)	Tail lead (190°)	Tail lead (175°)	Head lead (10°)	Head lead (10°)	Head lead (10°)	Perpendicular (90°)	Sperm head (N/A)
Total travel time (s)	0.593	0.542	0.523	0.560	0.584	0.518	0.532	0.619
Number of rotations	3	1	0	2	2	0	0.5	11
Rotation time ratio (distance)	11.8 (13) %	4.1 (7.6) %	0 (0) %	10.7 (11.1)%	3.9 (8) %	0 (0) %	47.7 (~16) %	Tumbling
Aligned time ratio (distance)	89 (87)	96 (93.4)	100 (100)	89.3 (88.9)	96.1 (92)	100 (100)	52.3 (~84)	N/A (Tumbling)
Final alignment with θ[b]	Head lead (~10°)	Head lead (~2°)	Tail lead (~10°)	Heard lead (~1°)	Head lead (~10°)	Head lead (0°)	Head lead (~20°)	N/A
Final location of head[a]	60 μm	105 μm	70 μm	35 μm	110 μm	77 μm	47 μm	15 μm

The simulation of the SLP with different initial position (Case 1–Case 7) and the simulation with a sperm head-like particle (Case 8)

[a]The particle location is measured as the distance from the inner wall of the channel

[b]The alignment angle "θ" is the angle between the primary flow direction and the SLP tail (Fig. 4)

4.2 Experimental confirmation of SLP alignment behavior

Using the inverted microscope (Nikon, A1), we were able to image individual sperm cells as they travelled through the spiral channel. In Fig. 5-1, a polar plot is used to represent the alignment of each measured sperm cell, and Fig. 5-2 and -3 shows two example images from which sperm cells were identified (among 102 cases). The results show a strong preference towards alignment and a weak preference towards the tail lead position (Fig. 5-1). Since the chance of having clearly identified sperm in each frame was entirely random, the alignment data collection can be used to reliably represent the general behavior of the sperm cell population. This result demonstrates that the self-alignment of sperm is a genuine phenomenon.

4.3 Improved focusing behavior: beads and sperm cells

With the three flow rates of 0.52 ml/min, 1.04 ml/min, and 1.7 ml/min the flow focusing behavior of 3 μm microbeads, 5 μm microbeads, and DAPI-stained sperm, was observed near the outlet of the spiral channel; the images and intensity plots are shown in Fig. 6. At the lowest flow speed, only the 5-μm beads are focused, and increasing the flow rate increases the focusing of the 3 μm beads and sperm cells, whose peaks appear sequentially from the inner to outer wall. These data appear to validate our hypothesis that the alignment behavior of the sperm cells in the channel would cause them to focus in a manner more similar to smaller particles, which is true both in terms of their location and the flow rate required to focus on them.

In Fig. 6a, the intensity percentile plot clearly shows different flow focusing behavior among the three different particles. Consistent with the theory, the 5-μm beads are found to be focused into a tight stream. Quantitatively, the 5-μm beads are found to focus at a position about 25% of the way across the channel into a tight peak that occupies less than 10% of the channel width (quantified at half-height). The 3-μm beads and sperm cells show very minimal tendency towards focusing, with a peak width spanning greater than 40% of the width in both cases (Table 2-1). Essentially, we observe that the 3-μm beads and sperm cells are not significantly focused at this lowest flow rate.

Figure 6b shows the focusing of particles at the flow rate of 1.04 ml/min which demonstrated an improvement of flow focusing of all particle cases relative to the slower flow rate of 0.52 ml/min. The most distinct improvement in flow focusing is in the 3-μm beads, whose stream width is now only ~10% of the channel's width, nearly a 4× improvement in flow focusing (Fig. 6b-4). These data imply that the forces created at this flow rate have led to flow focusing of the 3-μm beads, although they have not led to the complete flow focusing which occurs only at a higher flow rate (Fig. 6c). The flow focusing of sperm cells also improves at this higher flow rate, although the improvement is slight, with the new stream width occupying ~37% of the channel. The focused

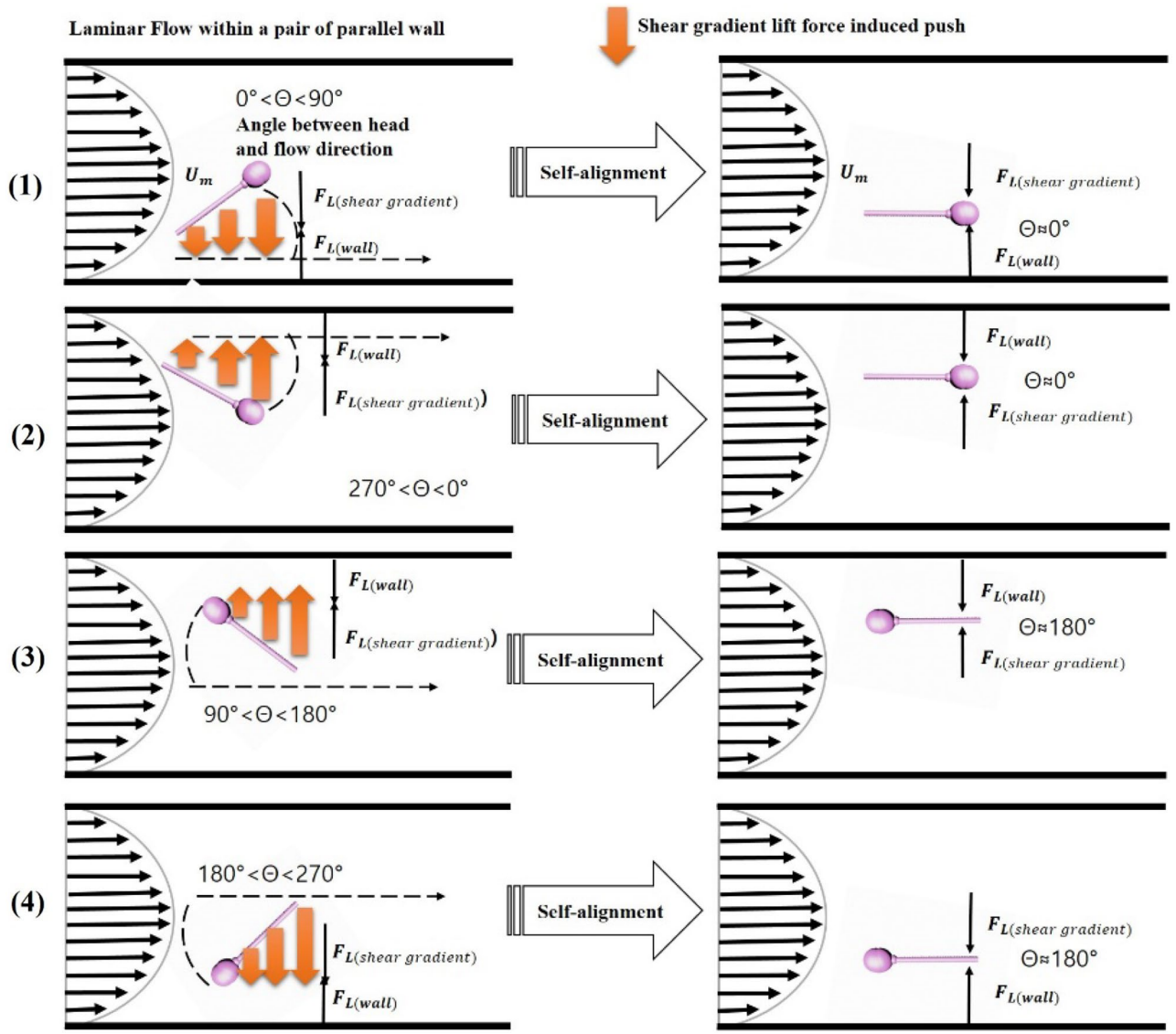

Fig. 4 SLP alignment behavior summary between a pair of parallel walls, (1) head leading with flow direction case, $0° < \theta < 45°$, (2) head leading with flow direction case, $310° < \theta < 0°$ (3) tail leading with flow direction case, $135° < \theta < 180°$, (4) tail leading with flow direction case, $180° < \theta < 225°$

stream of 5 μm beads is slightly changed in both width and position to the stream at the lower flow rate (~22% of the way across the channel, ~7% of the channel width) (Table 2-2). Although the flow focusing is not as evident in this case as in the faster case, the ordering of the beads in terms of size can already be seen and is the mechanism by which separation is achieved. Here though, the ordering of the peaks can also be used as evidence that, from the perspective of the flow, the sperm cells are acting like particles that are smaller than the 3-μm beads, which is especially interesting because the sperm cell's smallest dimension is ~3 μm.

Figure 6c shows the behavior of the three particles at the increased flow rate of 1.7 ml/min. As predicted by the theory, the flow focusing of 3 μm beads is very tight at the higher flow rate with a width equivalent to only ~7% of the channel width. With the flow rate increased to focus on smaller particles, the sperm cells have also focused much more tightly. Quantitatively, the width of the sperm cell stream is 25% of the channel width, which represents nearly a 2× improvement in focusing relative to the base case of 0.52 ml/min. Although the flow focusing of the 5-μm beads has diminished slightly with the increased flow rate, the stream width is still only ~12% of the channel width and is still tight enough to separate the 5-μm beads from other particles (Table 2-3). The sequential peaks, moving from the inner to outer wall as the apparent particle diameter decreases, are even more apparent at the higher flow rate (Fig. 6a–c-4).This observation implies that approximating

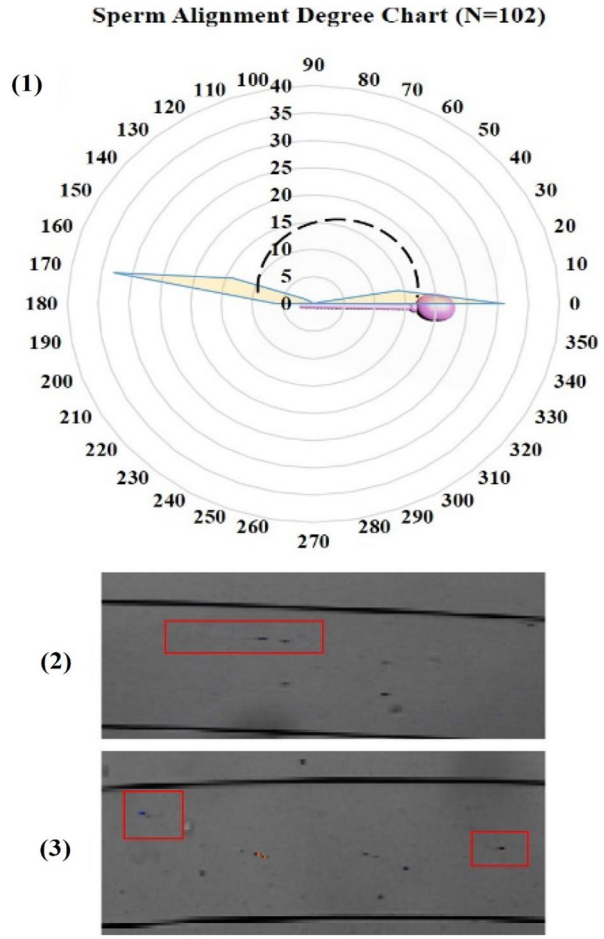

Fig. 5 (1) The polar plot of sperm alignment within the spiral channel, (2–3) identified sperm cell samples from a single frame of recorded high-speed video

the sperm cells as a sphere for use with present Dean flow theory requires using a representative diameter smaller than 3 μm, which would require an even faster velocity to achieve better flow focusing. We were not able to perform experiments at higher flow rates, as the required pressure was found to cause failure in our devices.

4.4 Improved focusing utility: simulated μTESE

The application that drove our interest in this problem is the separation of sperm cells from digested testicular biopsy samples that are obtained as part of a treatment for infertile men. The goal of improving the flow focusing of sperm cells was twofold: (1) improve the separation by selecting a smaller portion of the RBCs, and (2) increase the concentration of sperm cells in the final output by selecting a smaller portion of the total channel width. The optimal device operation would result in two, sharp, well-separated streams:one of RBCs and one of sperm cells. The results of this work helped us move much closer to this type of performance as we increased the operational flow rate from 0.52 to 1.7 ml/min.

For the 0.52-ml/min case, RBCs were focused in a sharp stream near the inner wall area of the channel (Fig. 7a-1, 3) that occupies less than 6% of the channel width (measured at half-height). However, sperm cells did not show a clear noticeable flow focusing trend (Fig. 7-1, 2), with a stream width of sperm greater than 40% of the channel width (Table 3-1), as before. This behavior is consistent with our previous result and leads to an operation in which, instead of selecting for the sperm cells, we select for and remove the RBCs. The RBCs advantageously focused to an inner middle portion of the channel where a waste selection can be made on the inner 35% of the channel to remove the vast majority of the RBCs (the small secondary peak impedes our ability to remove all of the RBCs). In this operation, it may be possible to flow the waste portion of the first run through the device again to try to recover the small quantity of sperm cells that would be selected in this stream, but this would only exacerbate the problem inherent in this operation: the sperm are of necessity suspended in a very large volume at a very low concentration.

At a flow rate of 1.04 ml/min, the trend of flow focusing of sperm cells was improved relative to the 0.52-ml/min case, although the ability to separate this stream from the stream of RBCs was diminished (Fig. 7a, b). The stream width of sperm cells is reduced to less than 30% of the channel width (Table 3-2), reduced by over a quarter width from the results at a lower flow rate (Fig. 7b-1, 2, 4). The sperm cells focus onto two peaks near the middle of the channel, the higher of which is located ~60% of the way towards the outer wall of the channel. Meanwhile, the focused stream of RBC has shifted toward the middle area of the channel and the secondary peak has become more pronounced (Fig. 7b-1, 3, 4). Overall, the stream width has increased to ~20% of the channel, and the stream is now centered about 46% of the way across the channel. This leads to quite considerable and disadvantageous overlap as half of the primary RBC peak was overlapped by about 25% of the sperm peak (Fig. 7b-4). Thus, this flow rate is found to be too high to tightly focus RBCs, and not high enough to create flow focusing of sperm cells.

In the 1.7-ml/min case (Fig. 7c), the focused stream of sperm cells was significantly improved compared to the previous flow rate cases. The stream width of sperm cells was ~22% of the channel width, about half of the width of the original unfocused stream width from the 0.52-ml/min case (Table 3-1, 3). The highest signal intensity is measured 60% of the way across the channel, although a fairly distinct secondary peak is present near the middle of the channel. The RBCs focused onto a tight stream occupying ~7% of the channel width and located ~44% of the way across the

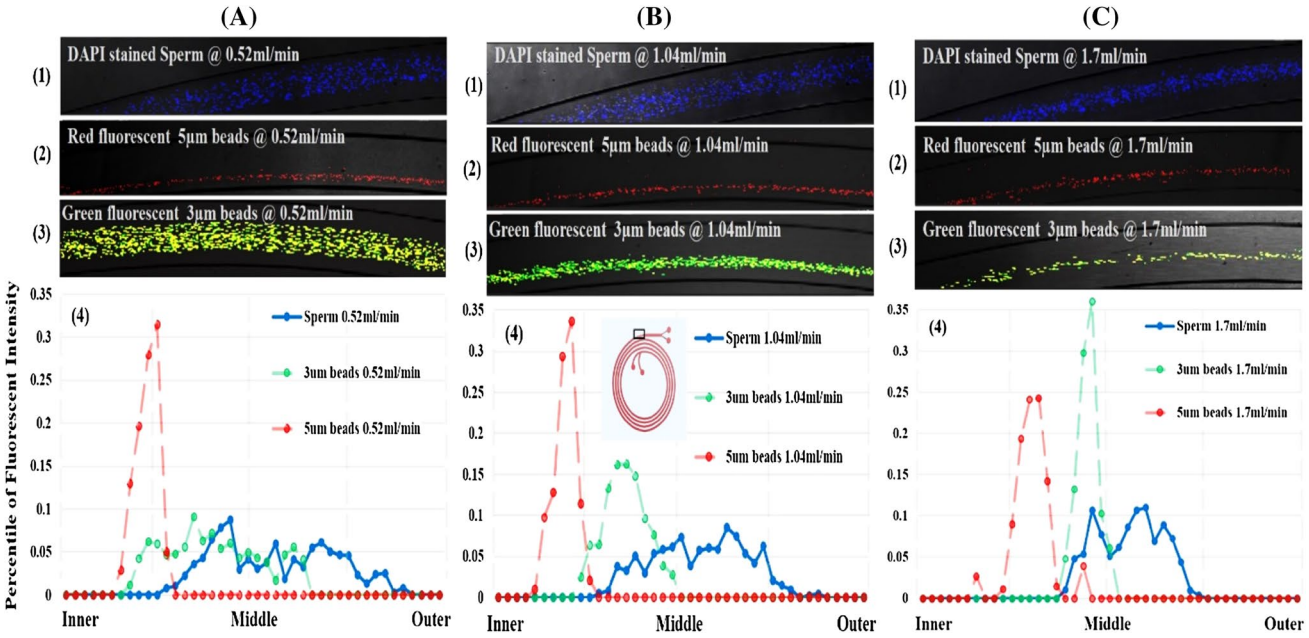

Fig. 6 Imaging results of DAPI-stained sperm, ~5 μm, and ~3 μm diameter beads at a flow rate of 0.52 ml/min (**a**), 1.04 ml/min (**b**), 1.7 ml/min (**c**). (1) projection image of DAPI-stained sperm, (2) projection image of 5 μm fluorescent beads, (3) projection image of 3 μm fluorescent microbeads, (4) fluorescent intensity percentile plot of all three types of particle

channel, although a much smaller secondary peak appeared close to the middle outer area of the channel which made a slight overlap (less than 30%) between a minor sperm peak and a major RBC peak (Fig. 7c-4). This flow rate offers the best possibility of selecting the sperm in a small volume.

The new particle model-based method clearly improved the flow focusing of sperm cells. However, the newly calculated flow rate also caused the focused stream to shift toward the middle of the channel. The shift should be caused by a combination of Dean drag force and the particle's movement to reach an equilibrium position between where the shear gradient lift force and wall wall-induced lift force are balanced (Fig. 1, two equilibrium positions middle of near long face wall of rectangular shape channel). By considering this shift, it is possible to determine a much improved protocol which relies on the improvements offered by the improved focusing behavior reported here.

Table 2 Intensity profile plot analysis of sperm and microbeads (Fig. 6a-4, b-4, c-4) when the injection flowrate is 0.52 ml/min, 1.04 ml/min, and 1.7 ml/min, respectively

	Peak width[a]	Highest peak position[b]	Peak's middle position[b]
0.52 ml/min Case (1)			
Sperm	17/42	19th/42	23.5th/42
3 μm bead	18/42	15th/42	17.5th/42
5 μm bead	4/42	11th/42	10th/42
1.04 ml/min Case (2)			
Sperm	15/41	26th/41	23.5th/41
3 μm bead	4.5/41	15th/41	15th/41
5 μm bead	3/41	9th/41	8.5th/41
1.7 ml/min Case (3)			
Sperm	11/43	26th/43	24.3th/43
3 μm bead	3/43	20th/43	19.5th/43
5 μm bead	5/43	14th/43	13.5th/43

[a]The peak width is the number of points measured from the left initial location with half intensity of the highest intensity peak value to the final half intensity value of right end. The total points were there to show the span width compared to the total width of the channel

[b]The value in ( ) is the total number points of each plot from inner wall (1st data point) to outer wall (the last data point)

4.5 Sperm viability test results

We were also able to observe that operating the spiral device at the higher flow rates suggested by this work did not cause catastrophic biological or physical damage to the cells. This is true both in terms of sperm viability (live/dead) and sperm morphology. In terms of the live sperm count, (Fig. 8-1) there is only a small difference (− 11 sperm and + 1 sperm) between the control and processed samples. This difference is especially minor when compared with the natural decay of sperm cells during clinical processing (Garrett et al. 2005). In terms of morphology, both the normal sperm head and normal sperm tail counts (Fig. 8-2, 3) suggest that the device does not impose excessive physical damage to the sperm

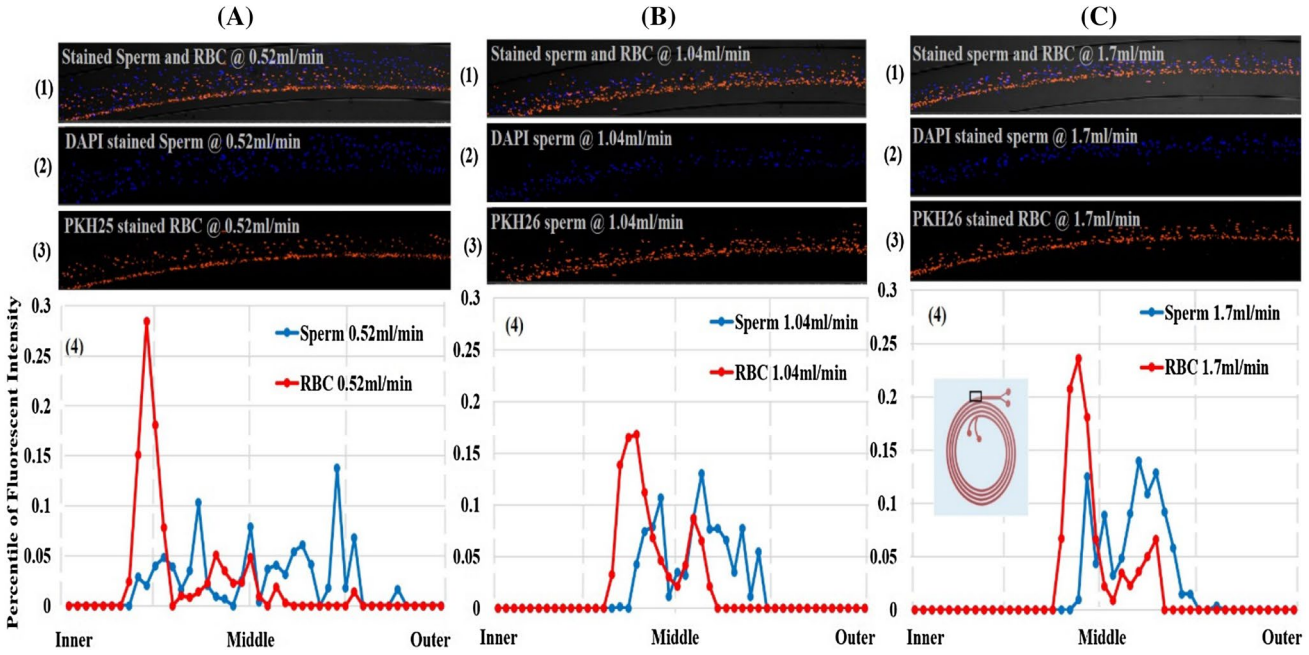

Fig. 7 Characteristics of stained simulated μTESE at a flow rate of 0.52 ml/min (**a**), 1.04 ml/min (**b**), and 1.7 ml/min (**c**)—(1) Projection image of DAPI-stained sperm and PKH26-stained RBC, (2) Sperm projection image (3) RBC projection image, (4) fluorescent intensity percentile plot of both types of particle

cells. The morphological differences between the control and processed samples, both in terms of the head and tail morphologies, are likely to be considered minor from the clinical perspective due to the high variability inherent in the morphology test's manual cell count methodology. The counts provide initial evidence that the new protocol is unlikely to damage the sperm during processing. Overall, viability and morphology tests suggest that the device operation with an increased flow rate has only a minor effect on the sperm cells.

Table 3 Intensity profile plot analysis of simulated μTESE sample test (Fig. 7a-4, b-4, c-4) when the injection flowrate is 0.52 ml/min, 1.04 ml/min, and 1.7 ml/min

	Peak width[a]	Highest peak position[b]	Peaks middle position[b]
0.52 ml/min Case (1)			
Sperm	18.5/(44)	32th/(44)	25.7th/(44)
RBC	2.5/(44)	10th/(44)	10th/(44)
1.04 ml/min Case (2)			
Sperm	13/(46)	26th/(46)	23th/(46)
RBC	9.5/(46)	18th/(46)	21.5th/(46)
1.7 ml/min Case (3)			
Sperm	10/(45)	27th/(45)	25th/(45)
RBC	3/(45)	20th/(45)	20th/(45)

[a]The peak width is the number of points measured from the left initial location with half intensity of the highest intensity peak value to the final half intensity value of right end. The total points were there to show span width compared to total width of the channel

[b]The value in () is the total number points of each plot from inner wall (1st data point) to outer wall (the last data point)

5 Conclusion

In conclusion, modeling and experimental results enabled the improvement of sperm and blood cell separations. Initially, we used a modeling approach to demonstrate the alignment behavior of sperm in the spiral channel. The modeling was completed with a 2D COMSOL® simulation and follow-on experimental studies of SLP behavior in a curved channel verified these results. The SLP behavior study showed that the particle would not continuously rotate while it was traveling through the curved channel and that the particle is mostly aligned with the primary flow direction either in a tail lead or a head lead position. This behavior was also confirmed by observing the alignment angle of all recognizable sperm cells with high-speed imaging near the outlet area of the spiral channel. Due to the SLP's alignment, the lateral migration-inducing forces (F_L and F_D) act over a smaller effective surface than is suggested by the rotating particle model.

A series of experiments with sperm cells and microbeads showed clear improvement between the new model and the previous approach. Analysis of projection images

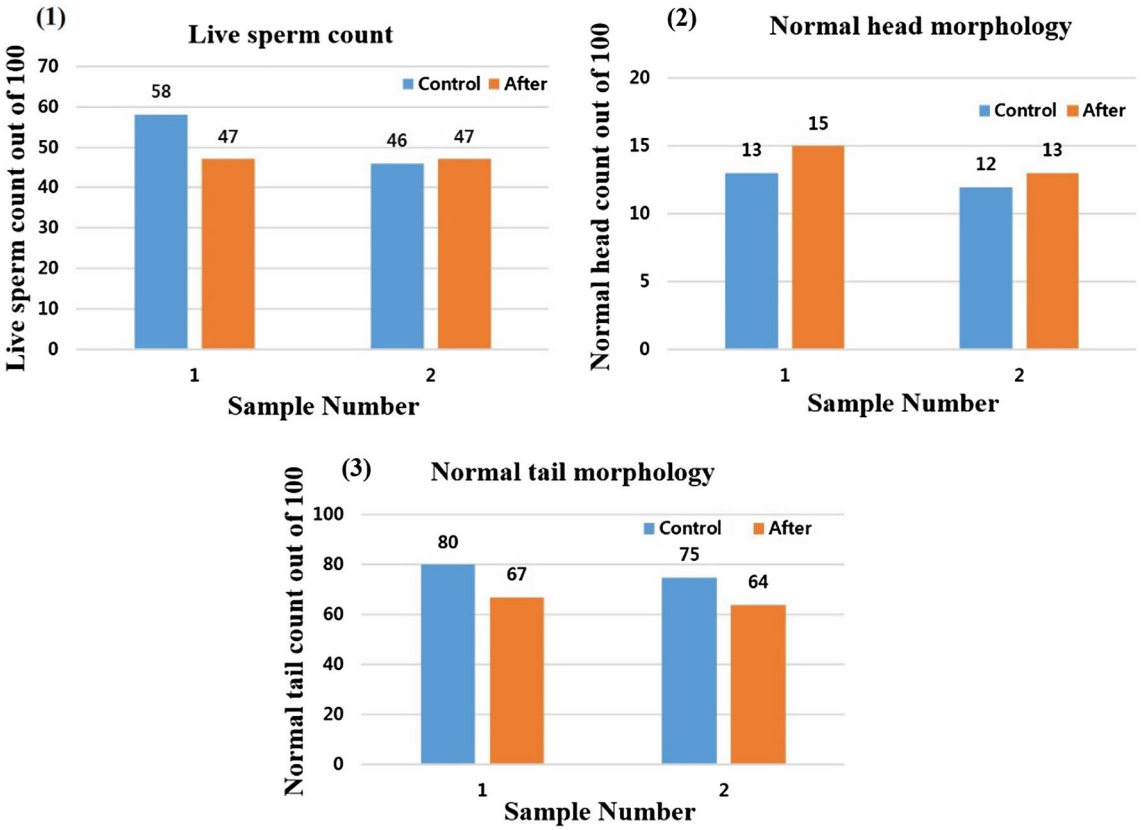

Fig. 8 Results of experiments measuring the biological influence of device operation, (1) live sperm count from live/dead test of two different samples, (2) normal head morphology count from morphology test of two different samples, (3) normal tail morphology count from morphology test of two different samples

from recorded high-speed videos confirmed that the flow focusing behavior (in required flow rate and position) of sperm was more similar to the 3-μm microbeads than to the 5-μm beads and that sperm cells may act like particles even smaller than the 3-μm beads. The improved protocol also improved separation of sperm from simulated μTESE samples. The flow focusing of sperm cells and RBCs was significantly improved compared to our previous reports (Son et al. 2015, 2017), which was confirmed by analysis of the projection image from recorded videos. The focused sperm cell stream appeared in the middle area of the channel and the focused RBCs stream appeared at the mid-inner wall area of the channel. However, there was still a slight overlap between the sperm cells and the RBCs, which would prevent complete separation.

A biocompatibility test shows the biological/physical effects of the new protocol. Two semen samples were utilized to conduct survival and morphology tests according to WHO guidelines. The live and normal shape sperm count results show that there were only minor changes in the quantities of living and normal sperm cells between control and processed samples. This means there was almost no significant negative effect from the new approach. Overall, the new understanding of SLP behavior when flowing in a curved channel provides improved sperm modeling, allowing a user to establish a protocol for sharper flow focusing of sperm cells. This new protocol can provide more precise sperm separation from μTESE samples, which should reduce clinical sperm search efforts significantly when compared to the conventional method that uses unprocessed samples. The simple biocompatibility study also gives us promising evidence that the approach can be used safely in a clinical setting.

Acknowledgements This material is based upon work supported by the National Science Foundation under Grant IIP-1549659. The authors would also like to thank the University of Utah Andrology program for their support.

Compliance with ethical standards

Conflict of interest Authors B.K.G., D.C., and J.H. declare a financial interest in a company, Nanonc, which holds an intellectual property license related to the technology described in this paper.

References

Amini H, Lee W, Carlo DD (2014) Inertial microfluidic physics. Lab Chip 14(15):2739–2761

Andersson H, Van den Berg A (2003) Microfluidic devices for cellomics: a review. Sens Actuators B Chem 92(3):315–325

Bhagat AAS, Bow H, Hou HW, Tan SJ, Han J, Lim CT (2010) Microfluidics for cell separation. Med Biol Eng Comput 48(10):999–1014

Bhagat AAS, Hou HW, Li LD, Lim CT, Han J (2011) Pinched flow coupled shear-modulated inertial microfluidics for high-throughput rare blood cell separation. Lab Chip 11(11):1870–1878

Cho BS, Schuster TG, Zhu X, Chang D, Smith GD, Takayama S (2003) Passively driven integrated microfluidic system for separation of motile sperm. Anal Chem 75(7):1671–1675

Diez-Silva M, Dao M, Han J, Lim C-T, Suresh S (2010) Shape and biomechanical characteristics of human red blood cells in health and disease. MRS Bull 35(5):382–388

Garrett C, Liu DY, McLachlan RI, Baker HWG (2005) Time course of changes in sperm morphometry and semen variables during testosterone-induced suppression of human spermatogenesis. Hum Reprod 20(11):3091–3100

Gossett DR et al (2010) Label-free cell separation and sorting in microfluidic systems. Anal Bioanal Chem 397(8):3249–3267

Guz N, Dokukin M, Kalaparthi V, Sokolov I (2014) If cell mechanics can be described by elastic modulus: study of different models and probes used in indentation experiments. Biophys J 107(3):564–575

Hur SC, Choi SE, Kwon S, Di Carlo D (2011) Inertial focusing of non-spherical microparticles. Appl Phys Lett 99(4):1–4

Kim SM, Lee SH, Suh KY (2008) Cell research with physically modified microfluidic channels: a review. Lab Chip Miniat Chem Biol 8(7):1015–1023

Ko Y-J, Maeng J-H, Lee B-C, Lee S, Hwang SY, Ahn Y (2012) Separation of progressive motile sperm from mouse semen using on-chip chemotaxis. Anal Sci 28(1):27–32

Koyama S, Amarie D, Soini HA, Novotny MV, Jacobson SC (2006a) Chemotaxis assays of mouse sperm on microfluidic devices scientists involved in reproductive science. Understanding. Anal Chem 78(10):3354–3359

Koyama S, Amarie D, Soini H (2006b) Chemotaxis assays of mouse sperm on microfluidic devices. Anal Chem 78(10):3354–3359

Lee MG, Shin JH, Bae CY, Choi S, Park JK (2013) Label-free cancer cell separation from human whole blood using inertial microfluidics at low shear stress. Anal Chem 85(13):6213–6218

Lin Y, Chen P, Wu R, Pan L, Tseng F (2013) Micro diffuser-type movement inversion sorter for high-efficient sperm sorting. In: International conference on nano/micro engineered and molecular, pp 7–10

Mach AJ, Carlo D (2010) Continuous scalable blood filtration device using inertial microfluidics. Biotechnol Bioeng 107(2):302–311

Martel JM, Toner M (2012) Inertial focusing dynamics in spiral microchannels. Phys Fluids 24(3):32001

Martel JM, Toner M (2013) Particle focusing in curved microfluidic channels. Sci Rep 3:1–8

Mossman JA, Pearson JT, Moore HD, Pacey AA (2013) Variation in mean human sperm length is linked with semen characteristics. Hum Reprod 28(1):22–32

Nagrath S, Sequist LV, Maheswaran S, Bell DW, Irimia D, Ulkus L, Smith MR, Kwak EL, Digumarthy S, Muzikansky A, Ryan P, Balis UJ, Tompkins RG, Haber DA, Toner M (2007) Isolation of rare circulating tumour cells in cancer patients by microchip technology. Nature 450:1235–1239

Nam J, Lim H, Kim D, Jung H, Shin S (2012) Continuous separation of microparticles in a microfluidic channel via the elasto-inertial effect of non-Newtonian fluid. Lab Chip 12:1347

Schuster TG, Cho B, Keller LM, Takayama S, Smith GD (2003) Isolation of motile spermatozoa from semen samples using microfluidics. Reprod Biomed Online 7(1):75–81

Shields CW IV, Reyes CD, López GP (2015) Microfluidic cell sorting: a review of the advances in the separation of cells from debulking to rare cell isolation. Lab Chip 15(5):1230–1249

Son J, Murphy K, Samuel R, Gale B, Carrell D, Hotaling J (2015) Non-motile sperm cell separation using a spiral channel. Anal Methods 7:8041–8047

Son J, Samuel R, Gale BK, Carrell DT, Hotaling JM (2017) Separation of sperm cells from samples containing high concentrations of white blood cells using a spiral channel. Biomicrofluidics 11(5):1–11

Suh RS, Zhu X, Phadke N, Ohl Da, Takayama S, Smith GD (2006) IVF within microfluidic channels requires lower total numbers and lower concentrations of sperm. Hum Reprod 21(2):477–483

Swain JE, Lai D, Takayama S, Smith GD (2013) Thinking big by thinking small: application of microfluidic technology to improve ART. Lab Chip 13(7):1213–1224

Uspal WE, Burak Eral H, Doyle PS (2013) Engineering particle trajectories in microfluidic flows using particle shape. Nat Commun 4:2666

WHO (2010) Examination and processing of human semen, vol. Edition, F.

Xie L et al (2010) Integration of sperm motility and chemotaxis screening with a microchannel-based device. Clin Chem 56(8):1270–1278

Zhou J, Papautsky I (2013) Fundamentals of inertial focusing in microchannels. Lab Chip 13(6):1121–1132